SAND87-0293C
Unlimited Distribution
Printed January 1988

Distribution
Category UC-70

DRYING OF AN INITIALLY SATURATED FRACTURED VOLCANIC TUFF

A. J. Russo and D. C. Reda
Sandia National Laboratories
Albuquerque, New Mexico

ABSTRACT

The isothermal drying of an initially saturated welded tuffaceous rock was studied experimentally. Gamma-beam densitometry was used to measure the material's effective porosity distribution prior to the drying experiment. It was then used to measure liquid saturation distributions during a 1400 hour drying period. The core selected for study was taken from the Busted Butte outcrop at the Nevada Test Site, part of the Topopah Spring Member of Paintbrush tuff. This specimen contained several microfractures transversely oriented to the direction of the water or vapor migration. These fractures were found to be regions of rapid dryout or low saturation even though they were displaced from the surface over which dry nitrogen was flowing. An imbibition experiment was performed earlier on the same core. In the imbibition experiment the presence of most of these microfractures was detected by discontinuities in the measured saturation curves, which indicated a delay in liquid transport past the microfractures.

NOMENCLATURE

C	beam contrast (I_{dry}/I_{wet})
D	core diameter
$\|ds\|$	uncertainty in measured saturation
I	beam intensity
I_o	initial beam intensity
L	core length
M	mass flow rate
q	gas volume flow rate
R	measured count rate
S	liquid saturation
T	temperature
t	time
x	axial coordinate
z	beam pathlength in material

Greek

μ	linear attenuation coefficient
ρ	vapor density
τ	electronic system time constant
ϕ	effective porosity

Subscripts

dry	at S=0 state
H_2O	value for water
i	material i
wet	at S=1 state
vin	vapor flow at end-plug

INTRODUCTION

Theoretical and experimental investigations of the technical feasibility of nuclear waste isolation within proposed geologic repositories are being done (1). The Nevada Nuclear Waste Storage Investigations (NNWSI) Project is addressing the feasibility of isolating heat-producing waste canisters at Yucca Mountain, Nevada, within tuffaceous rocks located above the water table. To accomplish this task, the physics of two-phase flows (of water and water vapor) through partially saturated tuff are being studied. In the near-field region flow may be driven by coupled thermal/hydrological processes and in the far-field, flow may be driven by purely hydrological processes (e.g., infiltration, fracture flows, or imbibition into the matrix material). Hydrological mechanisms would also dominate in the near-field region after the initial, high-heat-load period had passed.

In this investigation, the isothermal drying of an initially saturated core of tuffaceous rock was studied experimentally. This study had three objectives: (1) to obtain measurements that would aid in understanding the physical mechanisms of drying in a fine-pore fractured medium; (2) to use these measurements to help characterize the geologic medium from which the core was taken; and (3) to provide data that would be useful in the evaluation of numerical models.

EXPERIMENTAL METHOD

Figure 1 shows a schematic of the experimental apparatus. A cylindrical core sample (described in the next section) was dried and then brought to saturation by driving water into both ends of the evacuated core under pressure (2). The core was mated to gold-plated copper end-plugs that had air passages machined for access to the end faces of the core; the entire column was then encased in a flexible, impermeable sleeve of polyvinylidene fluoride (Kynar) shrink tubing. Continuous metal bands were compression-fitted over the outer surface of the sleeve/end-plug at each end of the assembly. This compression seal was positioned over an inner o-ring-in-groove

seal to provide complete isolation between the cylindrical surface of the core sample and the environment.

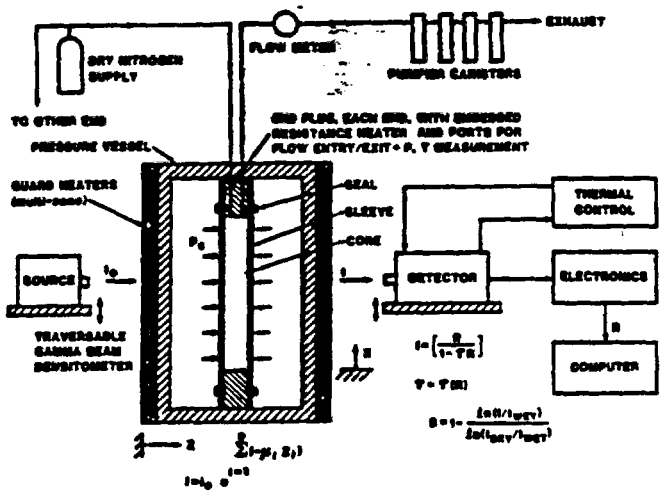

Figure 1 Schematic of Experiment

The core/end-plug assembly was positioned on the centerline of the test vessel, and the annular region surrounding it was filled with pressurized water at 5.5 MPa. This confining pressure was applied prior to saturating the core and was maintained throughout the imbibition and drying portions of the experiment. This pressure served to apply a net radial circumferential stress on the sample representative of the lithostatic loads at proposed repository depth, as well as to ensure that no flow bypass occurred between the outer surface of the rock and the inner surface of the confining sleeve. Miniature thermocouple beads were positioned every 2.75 cm along the outside of the sleeve to monitor the core axial temperature distribution. The entire test vessel was surrounded by a multizone guard heater, coupled by feed-back loops to thermal controllers. For the present experiment these heaters were not used.

Pressurized dry nitrogen from a regulated gas cylinder was fed into each end-plug (at 0.07MPa), past the end of the core in three 2.4-mm-wide circular grooves in the end-plug face and out of the same end-plug. This flow pattern exposed approximately 30% of the end face of the core to the flowing dry nitrogen. The nitrogen flowing out of each end-plug was fed into a serial bank of desiccant canisters (Matheson type 452 replaceable gas purifiers) and then vented to the room atmosphere. Each of the desiccant canisters was removed and weighed periodically to determine the mass of water that had evaporated from the core since the previous measurement. The desiccant canisters were changed often enough so that the last canister in the series always registered a negligible weight gain, which ensured that virtually all the water leaving the core was captured. The pressure and flow rate of the drying gas at each end of the core was monitored and recorded. To begin the experiment the gas flow rate was set at 5 standard cm^3/s. The initial weight loss measurements indicated a maximum evaporation rate of about 21 $\mu g/s$ from each end of the core. Using the equation,

$$\dot{M}_{vap} = \rho q \qquad (1)$$

where M_{vap} is the mass flow rate of water vapor from each end of the core, ρ is the density of vapor in the end-plug region, and q is the volume flow rate of the dry nitrogen, the density ρ can be calculated and the partial pressure of the vapor in the exiting gas (at room temperature=20°C in this case) can be determined. For the conditions indicated, this pressure was found to be approximately 550 Pa. Since the vapor pressure of water at 20°C is 2339 Pa, this gas flow rate was adequate to maintain a strong drying condition at the ends of the core. As the test progressed, the evaporation rate diminished to less than 2 $\mu g/s$, and the flow rate was reduced to 1.25 cm^3/s (after 39 days). This kept the exit vapor pressure to less than 200 Pa for most of the drying period. Figures 2 and 3 show the maximum vapor pressure at the end-plug exit for the top and bottom end-plugs, respectively. The fact that the vapor flow rates from the two core ends were slightly different indicates that there is some inhomogeneity in the core properties.

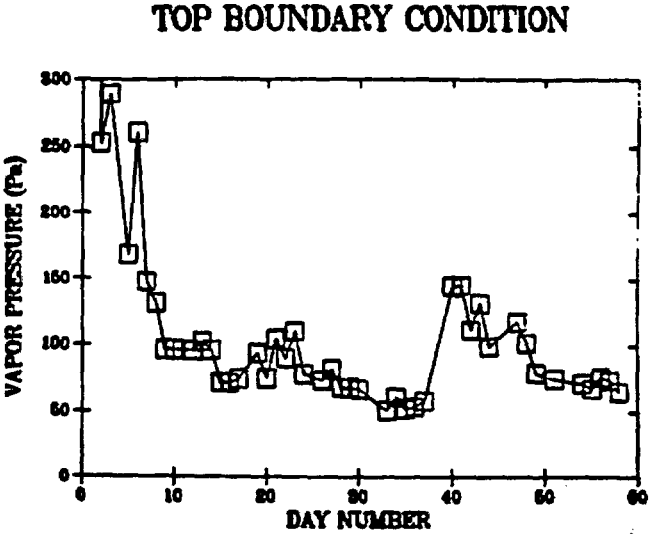

Figure 2 Maximum Vapor Pressure at the Upper End of the Core

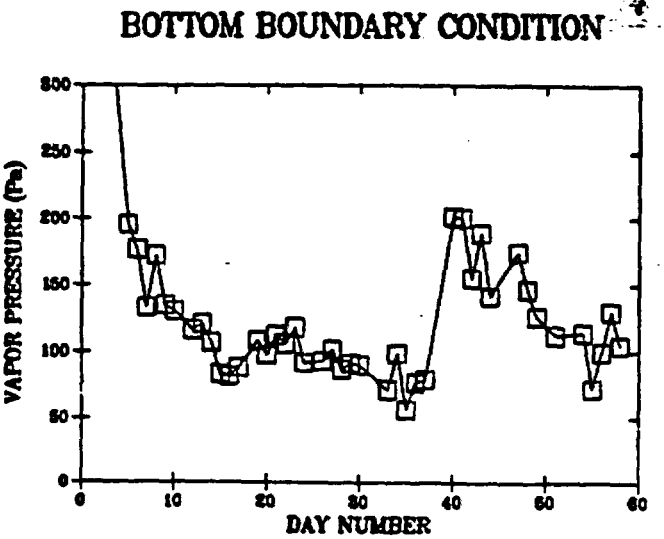

Figure 3 Maximum Vapor Pressure at the Lower End of the Core

The dry gas flow was continued for 58 days and the canister weight changes were recorded every one or two days. At each weighing period gamma-beam densitometer scans were taken along the centerline of the test vessel (and core) and compared with the "wet and dry" measurements to determine the saturation levels at each axial location as a function of time. A description of the gamma-beam calculations is given in Reference 2; however, a synopsis of that theory will be given here for completeness.

Gamma-beam densitometry relies on the attenuation and scattering of known-energy photons as they pass through matter (3). In

the present case, a cesium-137 pellet (5 curies) emitted 0.662 MeV photons from a source vault. These photons exited the source vault, through a 6.35-mm collimator tube, and passed through the pressure vessel and core sample. The reduction of the initial beam intensity, I_o, by scattering and absorption is described by Eq.(2).

$$I = I_o \exp\left[-\sum_{i=1}^{n} \mu_i z_i\right] \tag{2}$$

where I is the beam intensity of unattenuated photons exiting the test chamber and $\mu_i z_i$ is the product of the total linear attenuation coefficient, μ_i, and the path length, z_i, for material i (n is the total number of materials in the beam path).

After passing through the test fixture, gamma photons enter a detector vault through a collimator tube (also 6.35 mm) and strike a sodium iodide crystal to produce visible photons. These visible photons are detected by a photomultiplier tube, which, together with a built-in preamplifier, send a voltage pulse to counting electronics for each photon detected. The magnitude of this voltage pulse is proportional to the energy of the incoming gamma photon. A single-channel analyzer is then used to discriminate pulse height, yielding a count rate R (counts/second) proportional to the intensity of unattenuated photons, I. At high fluxes, some pulses "overlap" in time and are subsequently lost to the counting electronics. The conversion of the measurement R back to the intensity I is thus nonlinear, depending on the characteristic time constant τ of the detection system:

$$I = \frac{R}{1 - \tau R} \tag{3}$$

where $\tau = \tau(R)$ is a time constant function that must be obtained by calibration of the system electronics. Figure 4 shows a schematic of the "contrast calibration method" used.

CONTRAST METHOD FOR ELECTRONICS CALIBRATION

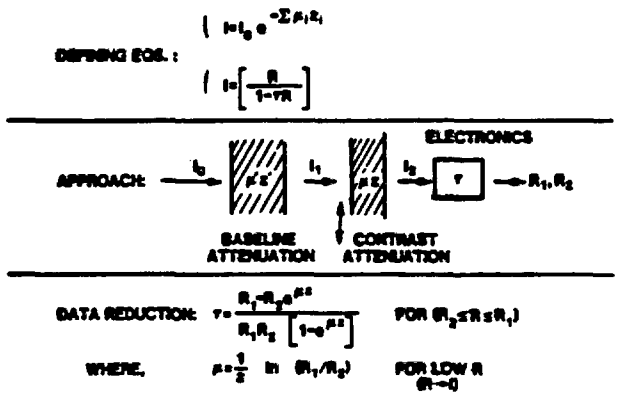

Figure 4 Contrast Method Schematic for Electronics Calibration

In that procedure, some "baseline" attenuation (by any material) produces an intensity I_1 and corresponding count rate R_1. The baseline intensity is then "contrasted" by the addition of a material of known thickness and composition to the beam path. In the present case, water (μ = 0.0853/cm) was used for the material of known composition, and aluminum blocks of varying thickness were used as the baseline material. A count rate, R_2, corresponding to the contrasted intensity I_2 ($I_2 < I_1$) is then measured.

By systematically changing the thickness of the baseline material(s), and by repeating the above procedure, data over the entire count rate regime of interest can be obtained. From Eqs. (2) and (3), the time constant (averaged between R_1 and R_2) at each point is

$$\tau = \frac{R_1 - R_2 e^{\mu z}}{R_1 R_2 (1 - e^{\mu z})} \tag{4}$$

where μz refers to the contrast material (water) and all other quantities on the right hand side are known.

A calibration curve for $\tau(R)$ can then be generated by curve-fitting the measured data. The curve used is shown in Figure 5 where the horizontal bars define the R_2 to R_1 range measured in each contrast test. All measurements taken during the drying experiments were in the range 13 to 15 kHz, and deadtime corrections were thus small.

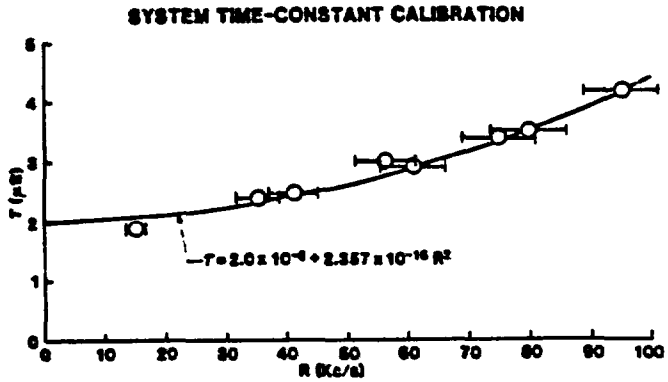

Figure 5 System Time-Constant Calibration Curve

In order to minimize signal drift effects, the crystal and photomultiplier tube (both housed in the detector vault) were held at a constant temperature (20 °C) by use of a cooling-coil and thermal bath flow loop. A reference attenuation measurement was taken at the start of each data scan by positioning the beam to penetrate the metal end-plug rather than the core sample. Any variations in signal level due to gain or source strength drift would thus be observed and accounted for in data reduction. Unfortunately, the room temperature could only be controlled to 20±3°C so that the small thermally-induced density changes in the system were not accounted for.

The procedure for using this instrumentation for measuring core porosity, ϕ, and liquid saturation, S, at each axial location can now be summarized. At each z: L location, the limiting dry and wet intensities were calculated from the measured count rate before and after imbibition, respectively. The contrast distribution, $C(z\ L) = I_{dry}/I_{wet}$, was stored on a disk file for later use. This total change in signal (dry to wet) is due solely to the filling of the core's effective porosity with a path length of liquid water equal to the product ϕD, where D is the core diameter. The attenuations caused by all the other materials in the beam path cancel out of the ratio (I_{dry} I_{wet}), yielding

$$\phi = \frac{\ln C}{\mu_{H_2O} D} \tag{5}$$

where the attenuation coefficient for water and the core diameter are both known. It follows from Eq. (2), that for any intermediate saturation $0 < S < 1$,

$$S = 1 - \frac{\ln(I/I_{wet})}{\ln(I_{dry}/I_{wet})} \tag{6}$$

Uncertainty in the measurement of S due to finite count times, denoted by $|ds|$, can be estimated from prior error analysis (4).

$$|ds| = \sqrt{Ri}(1 - \tau R) \ln C \cdot t^{-1} \tag{7}$$

In the present application R = 13 to 15 kHz, t, the counting interval at one scan point = 100 s, $(1 - \tau R) \approx 0.97$, and C = 1.05 to 1.10, defining a maximum uncertainty ds = 0.01 to 0.02. Because of room temperature variations and other drifts, the overall error was much higher than this (≈0.1); therefore, the following procedure was used to correct for thermal factors. The total moisture content of the core was calculated from the measured gamma-beam saturation values

and compared with the moisture content calculated from the weight loss measurements which were accurate to at least ±1%, and the reference count rate from the end-plug measurement was adjusted to bring the two values into agreement. The corrected saturation values were therefore valid to within 2%.

CORE CHARACTERIZATION

A block of densely welded tuff was taken from the Busted Butte outcrop at the Nevada Test Site (the Topopah Spring member of Paintbrush tuff). A series of adjacent core samples was drilled from this block and separate cores were used to make permeability and porosity measurements to characterize the matrix material. The liquid permeability of the unfractured matrix material was measured to be 3 to 5×10^{-19} m^2 independent of the temperature in the range 25 to 90°C (5). The gas permeability was measured as a function of average pore pressure by Reda (6); results showed gas permeability to be linearly proportional to inverse pore pressure (the Klinkenberg effect), from a value of 5×10^{-19}m^2 at "infinite" pressure to 5×10^{-18} m^2 at atmospheric pressure. On the basis of these results, and assuming a tortuosity factor of 5, the average pore diameter of the matrix material was estimated to be 8×10^{-9} m.

A cylindrical core 5.08 cm in diameter and 24.77 cm long was precision ground from the original rock specimen for use in the imbibition (2) and drying experiments. Visual inspection of this core showed it to contain a transverse microfracture near one end and a 10 cm long "altered zone" near the midcore region, where the densely welded matrix material changed from its basic brown/tan/pink coloration to a predominantly grayish coloration.

Attenuation measurements were made at uniform spacings of one beam diameter along the entire length of the core, defining a spatial resolution of $\Delta x/L = 0.0256$. A direct comparison of the dry and wet scans allowed the effective porosity distribution, $\phi(x/L)$, to be determined from Eq.(5). Results are shown in Figure 6.

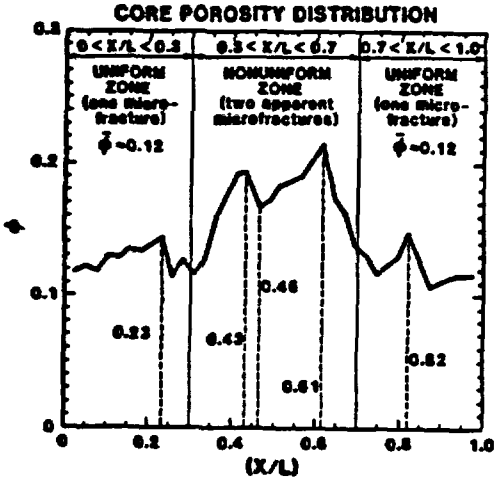

Figure 6 Core Porosity Profile from Gamma-Beam Measurements

Consistent with the results of the visual inspection, the core was found to have several distinctive zones and features. Two regions, each of length $|\Delta x/L| = 0.3$, originating at opposite ends of the core, were found to be of essentially the same average porosity ($\phi = 0.12$), the only apparent difference being the existence of a single transverse microfracture in the region, $0.7 < x/L < 1.0$ crossing the core centerline at $x/L = 0.82$. Since the gamma-beam diameter is much larger than any single microfracture such microfractures result in a spread out peak in intensity when they are encountered (7).

These observations indicate that (1) a beam defined porosity peak indicates the presence of a transverse microfracture plane (or a very thin layer of altered material) and (2) the beam crossed these features in an essentially edge-on orientation as it was traversed along the core centerline.

The altered zone in the central region of the core was found to have a higher effective porosity ($\phi \approx 0.18$) with two distinctive peaks, one at x/L = 0.43 and one at x/L = 0.61. These did not correspond to any visually observed fractures at the core surface; however, they did result in discontinuities in the progress of the wetting front during the imbibition experiment. The smaller peak, shown in Figure 6, at x/L = 0.23 did not correspond to any visible discontinuity, nor did it have any influence on the imbibition front; however, it did affect the saturation curve during drying in a similar way to the other apparent microfractures. Further observations of these apparent fracture regions are planned during posttest sectioning of the core.

EXPERIMENTAL RESULTS

A total of 45 saturation distribution scans and captured-vapor weight measurements were made over a 58-day drying period. The data aquisition time per core scan was ≈1 hour, with attenuation measurements being recorded at an axial spacing of one beam diameter ($\Delta x/L = 0.0256$). All data were assigned the time at the start of a scan; hence, the temporal resolution was to the nearest hour. Weight loss measurements were made on a Mettler type AE166 electronic balance to a precision of 1 mg.

The results of the captured-vapor weight loss measurements are shown in Figure 7. From the measured porosity data of the core and its known dimensions, the amount of water contained in the fully saturated core was estimated to be 75.4 g. A large fraction of this water (≈10%) was removed on the first day, with the bulk of it (7%) coming from the top end of the core. This end was found to be of *lower* permeability during imbibition. The reason for the difference in evaporation from the two core ends is not known, but the fact that a fracture zone was close to the top of the core may have influenced this asymmetry. After the first day, the weight loss rate slowed considerably, with evaporation from the bottom end of the core often slightly greater than that from the top. To avoid having to replace the dry nitrogen gas bottles too often, the gas flow rate was reduced from 5 cm^3/s on the first day to 4.2 cm^3/s on days 2 through 10, to 3.3 cm^3/s on days 11 through 17, to 2.5 cm^3/s on days 18 through 33, and 1.25 cm^3/s thereafter as the evaporation rate slowed. These changes in gas flow rate appeared to have no significant effect on the evaporation rate from either end of the core. The total average saturation of the core as a function of time is shown in Figure 8. This curve was used as a reference to correct for temperature-induced variations in the gamma-beam saturation data.

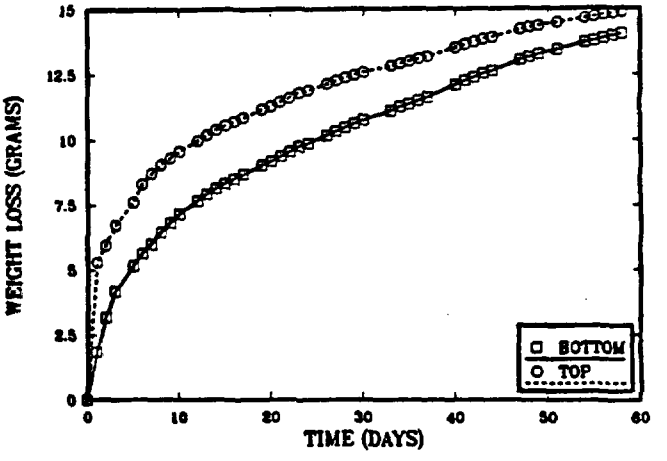

Figure 7 Rate of Water Removal from Each End of the Core

Figures 9 through 11 show the corrected saturation data along the axis of the core after the 2nd, 29th, and 58th days of drying. From Figure 9 it can be seen that almost immediately the saturation

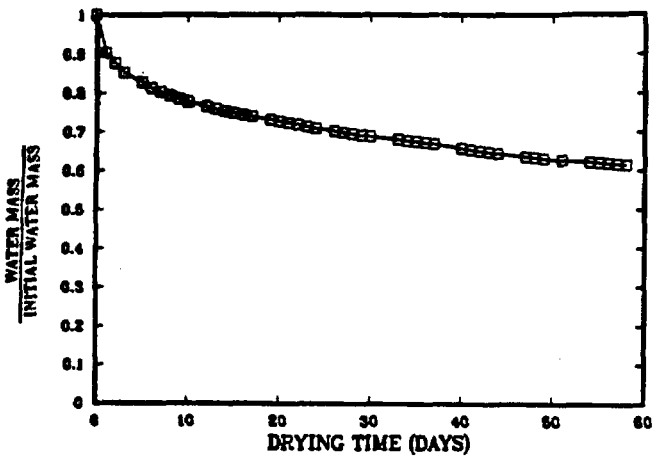

Figure 8 Average Core Saturation from Weight Loss Measurements

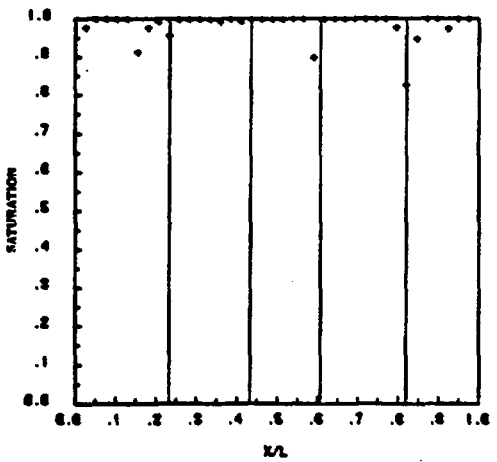

Figure 9 Core Saturation Profile from Gamma-Beam Measurements after 2 days

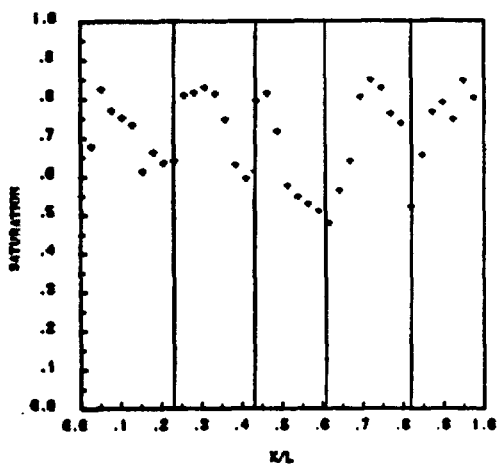

Figure 10 Core Saturation Profile from Gamma-Beam Measurements after 29 days

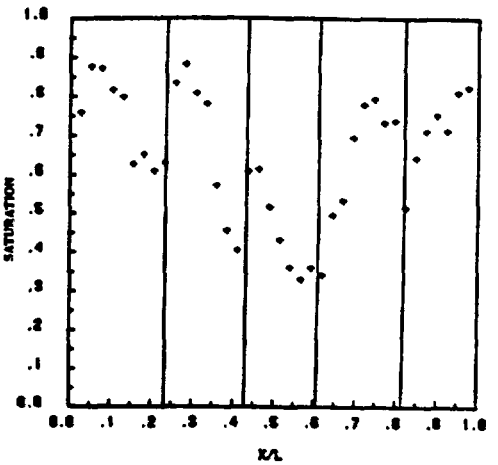

Figure 11 Core Saturation Profile from Gamma-Beam Measurements after 58 days

in the vicinity of the porosity peaks (microfractures) was reduced.[1] As time progressed (Figures 10–11) a lower saturation was always maintained in the same regions although the general saturation level was declining. Surprisingly the core seemed to be drying from the inside out since the lowest saturation levels occur near the center of the core. Since the porosity of the core was the highest in that region, it would be expected that the pore size might also be larger there and that capillary forces would tend to draw water into the end regions. An alternate possibility is that the very small pore sizes cause a reduction of vapor pressure in some regions and transport from the large to small pores occurs by evaporation, vapor diffusion, and condensation. At room temperatures, however, the vapor pressures (and vapor pressure gradients) are low, and diffusion rates are very slow, so this is not considered likely. A numerical model was used to simulate the experiment (8). The numerical model accounted for vapor diffusion and the results of the model indicated that vapor diffusion was very small. The calculated saturation profiles of the model agreed fairly well with the experimental observations except near the core ends, where the observed values remained higher than numerical predictions.

The fact that water can be transported from the interior of the core to the surface across microfractures raises some interesting questions about waste isolation calculations. For example, how fast will a tracer particle in the high porosity region take to migrate to the surface during drying? Future experiments will attempt to answer such questions.

CONCLUSIONS

During the isothermal drying process in small-pore tuffaceous rocks, the presence of microfractures and high porosity regions significantly affect the saturation distribution within the rock. These high-porosity regions appear to dry first even though they are internal to the core volume. This result was observed as the core saturation varies from 100% to 40% in the high porosity regions. Transport of water through the rock appears to be dominated by capillary flow of the liquid.

The rate of water vapor mass loss from the core was almost independent of the gas flow rate of the drying gas for this experiment which kept the maximum pressure of the vapor at the surface below 10% of the equilibrium vapor pressure at the core temperature.

[1] The absolute value of S in the fracture cannot be measured because the gamma beam diameter is much larger than the fracture width so that only some space-averaged quantity can be reported.

As a consequence of matrix material nonuniformities and the presence of microfractures, detailed characterization and modeling of transport through tuffaceous rocks on a submeter scale will be very difficult. Calculation of solute transport will be hampered by lack of information on the micro-mechanics of porous flow.

ACKNOWLEDGMENTS

This work was performed at Sandia National Laboratories supported by the U.S. Department of Energy under Contract Number DE-AC04-76DP00789.

The assistance of L. L. Schluter in the data acquisition and reduction and L. M. Powell in equipment fabrication is gratefully acknowledged.

REFERENCES

1. Roseboom, Jr., E. H., "Disposal of High-Level Nuclear Waste Above the Water Table in Arid Regions." U.S. Geological Survey Circular 903, 1983.
2. Reda, D. C., "Influence of Transverse Microfractures on the Imbibition of Water into Initially Dry Tuffaceous Rock." *Proc. of Symposium on Flow and Transport Through Unsaturated Fractured Rock, Amer. Geophysical Union Fall Meeting*. San Francisco, CA, Dec. 1986.
3. Hewitt, G. F., Measurements of Two Phase Flow Parameters. Academic Press, London, 1978.
4. Reda, D. C., Hadley, G. R., and Turner, J. R., "Application of the Gamma-Beam Attenuation Technique to the Measurement of Liquid Saturation for Two-Phase Flows in Porous Media." *Proceedings of 27th International Instrumentation Symposium, ISA*, Indianapolis, IN, 1981.
5. Reda, D. C., "Liquid Permeability Measurements on Densely Welded Tuff Over the Temperature Range 25° to 90°C." SAND85-2482, Sandia National Laboratories, 1985.
6. Reda, D. C., "Slip-Flow Experiments in Welded Tuff: The Knudsen Diffusion Problem." *Proceedings of International Symposium on Coupled Processes Affecting the Performance of a Nuclear Waste Repository, Lawrence Berkeley Laboratory, CA*, 1985.
7. Reda, D. C., and Russo, A. J., "Experimental Studies of Oil Withdrawal from Salt Cavities via Fresh-Water Injection," SAND83-0347, Sandia National Laboratories, 1984.
8. Bixler, N. E., Eaton, R. E., and Russo, A. J., "Drying Analysis of a Multiphase, Porous-Flow Experiment in Fractured Volcanic Tuff," in *Fundamentals of Heat Transfer in Drying*. (Joint ASME/JSME Meeting, Honolulu, Hawaii, March 22-27, 1987).

APPENDIX A

The data presented in this paper are compiled in the NNWSI Data Records Management System, File Number 51, LO7.A-12/04/85. No hydrologic property values were measured in the experiment described, and the data presented are not currently considered as information necessary to be entered into the NNWSI Science and Engineering Properties Data Base (SEPDP). If, at a future date, the data presented here are used in the validation of a computer code whose predictions may be used in repository licencing arguments, the data will be entered into the SEPDP.